ACS OMEGA

Open Access

http://pubs.acs.org/journal/acsodf

Article

Adsorption Behaviors and Mechanism of Phenol and Catechol in Wastewater by Magnetic Graphene Oxides: A Comprehensive Study Based on Adsorption Experiments, Mathematical Models, and Molecular Simulations

Yuhua Wu,[‖] Xi Zhang,[‖] Caizhu Liu, Lina Tian, Yufan Zhang, Meilin Zhu, Weiye Qiao, Jianbo Wu, Shu Yan, Hui Zhang, and Hongcun Bai*

Cite This: *ACS Omega* 2024, 9, 15101−15113

Read Online

ACCESS | Metrics & More | Article Recommendations | Supporting Information

ABSTRACT: This study provides a comprehensive analysis of the adsorption behaviors and mechanisms of phenol and catechol on magnetic graphene oxide (MGO) nanocomposites based on adsorption experiments, mathematical models, and molecular simulations. Through systematic experiments, the influence of various parameters, including contact time, pH conditions, and ionic strength, on the adsorption efficacy was comprehensively evaluated. The optimal contact time for adsorption was identified as 60 min, with the observation that an increase in inorganic salt concentration adversely affected the MGOs' adsorption capacity for both phenol and catechol. Specifically, MGOs exhibited a superior adsorption performance under mildly acidic conditions. The adsorption isotherm was well represented by the Langmuir model, suggesting monolayer coverage and finite adsorption sites for both pollutants. In terms of adsorption kinetics, a pseudo-first-order kinetic model was the most suitable for describing phenol adsorption, while catechol adsorption conformed more closely to a pseudo-second-order model, indicating distinct adsorption processes for these two similar compounds. Furthermore, this research utilized quantum chemical calculations to decipher the interaction mechanisms at the molecular level. Such calculations provided both a visual representation and a quantitative analysis of the interactions, elucidating the underlying physical and chemical forces governing the adsorption phenomena. The findings could not only offer crucial insights for the treatment of coal industrial wastewater containing phenolic compounds with bridging macroscopic observations with microscopic theoretical explanations but also advance the understanding of material−pollutant interactions in aqueous environments.

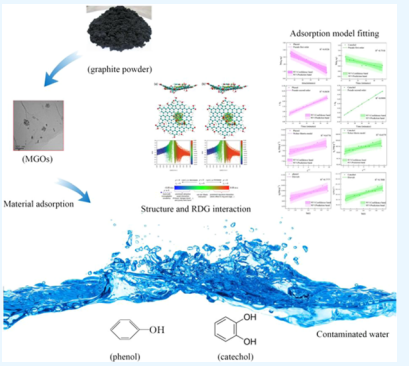

1. INTRODUCTION

The phenolic compounds are important organic pollutants produced in many chemical processes, such as petroleum refining, coal coking, gas refining, papermaking, and many fine chemical synthesis.[1,2] Phenol and its derivatives have the potential toxicity of carcinogenesis, teratogenesis and mutation and can be accumulated in the environment, which will cause great harm to human health, water environment ecology, and agriculture.[3−5] As a result, a large amount of phenol-containing wastewater from different chemical processes has been listed as toxic hazardous environmental pollutants. Therefore, the treatment of phenol-containing wastewater has become an important research topic widely concerned by both academia and industries.[6]

Because of the wide range of sources of wastewater containing phenols, the types and initial concentrations of phenols in water vary greatly. According to the difference of phenol concentration, it can be generally divided into high-concentration wastewater containing phenol (more than 1000 mg/L), medium-concentration wastewater containing phenol (5−500 mg/L), and low-concentration wastewater containing phenol for targeted treatment. For the middle- and high-concentration wastewater containing phenol, extraction, stripping, chemical precipitation, and other methods are usually used for the recovery and utilization of phenolic compounds.[7,8] However, due to the low phenol concentration, poor recovery economy, and large relative amount, the low-phenol wastewater is generally treated by catalytic degradation, biodegradation, adsorption, and other methods.[9−12] Because the chemical structure of phenolic compounds is difficult to degrade, the catalytic degradation and biodegradation methods generally need to go through multilevel treatment to complete, and the economic cost increases significantly with the

Received: November 23, 2023
Revised: February 23, 2024
Accepted: March 1, 2024
Published: March 23, 2024

https://doi.org/10.1021/acsomega.3c09346
ACS Omega 2024, 9, 15101−15113

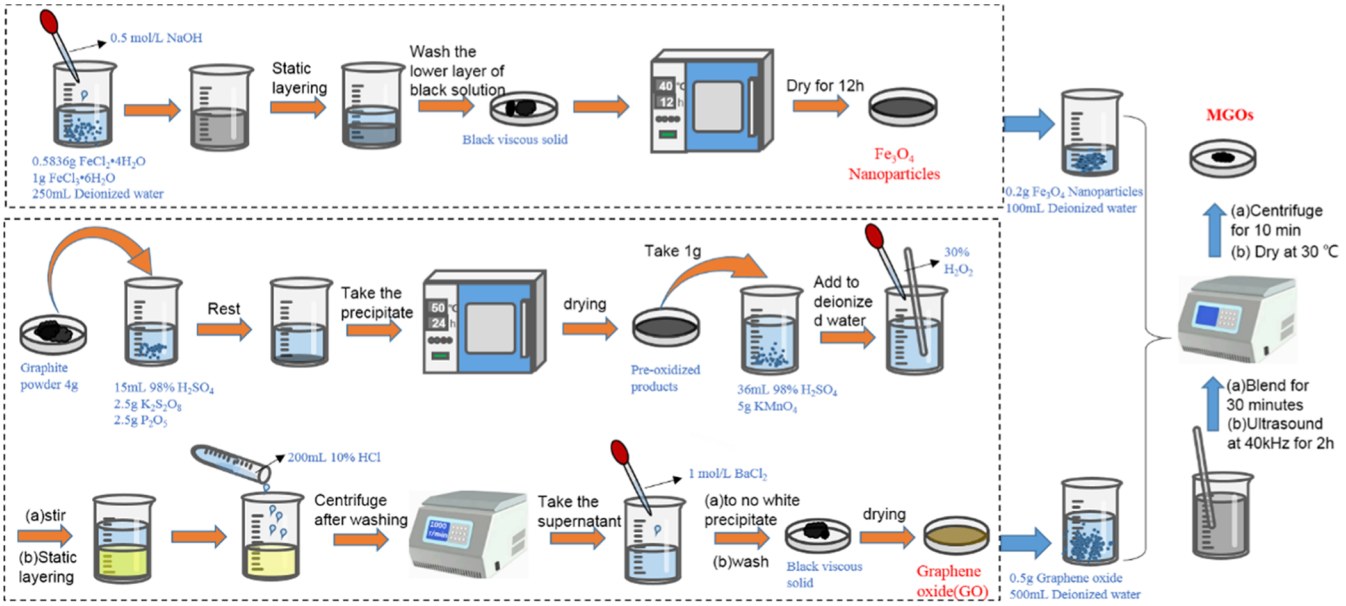

Figure 1. Details for the Preparation of MGOs.

extension of the treatment process.[13,14] As one of the most commonly used wastewater treatment methods, the adsorption method is also used in the treatment of phenol-containing wastewater.[15,16] At present, activated carbon, macroporous resin, and new carbon materials are also investigated for the adsorption and removal of phenolic compounds in wastewater.[17−19]

For the removal of toxic and harmful components in sewage by adsorption, the selection of adsorption materials is the key issue. In recent years, graphene (GR) and graphene oxides (GOs) have shown many advantages in the field of wastewater treatment due to the unique two-dimensional nanostructure, high surface area, high surface activity, and high oxygen-containing functional groups,[20−22] which have a potential application prospect. It should be pointed out that it is difficult to recover the adsorbed GOs in water and it is easy to cause secondary pollution. On the other hand, magnetic nanoparticles have the characteristics of large-scale controllable preparation and have intrinsic magnetism to make it easy to recover and reuse.[23] In addition, compared with other carbon-based materials, MGO has good adsorption properties. In 2020, Fang et al. conducted research on the adsorption of phenolic substances on carbon-based materials, including graphene, carbon nanotubes, graphite, and biochar. Graphene is rich in π-electrons, has a large specific surface area and electronic conductivity, and can easily achieve chemical functionalization. Therefore, graphene-based adsorbents have been shown to be effective in removing phenolic substances.[24] Cui et al. prepared a three-dimensional (3D) N-doped graphene oxide aerogel in 2023, and the adsorption capacity of phenol was roughly 24.28 mg/g.[25] In 2018, Vunain E[26] used low-cost activated carbon prepared by sunflower shell residue to remove catechol and resorcinol from aqueous solution in the adsorption experiment. The adsorption capacity of biological carbon for catechol was measured at about 100 mg/g. Therefore, magnetic graphene oxides (MGOs) can be prepared by combining magnetic nanoparticles with graphene oxides. The nanocomposites can retain the advantages of the two materials; at the same time, it is easy to recycle and reuse and effectively reduce the use cost.

In the current work, a new type of MGO material was synthesized by composite treatment based on the preparation of graphene oxide and nanometer Fe_3O_4 particles. The adsorption and removal of phenol and catechol in water were studied by using the MGO nanomaterials as adsorbents. The effects of the contact time, pH value, and ionic strength on the adsorption of phenol and catechol by magnetic graphene oxides were studied, and the isotherms and kinetic mechanism of the adsorption process were analyzed. Moreover, the molecular insights into the adsorptions of phenol and catechol over the surfaces of GOs are understood from quantum chemical viewpoints. We hope that the current work would be beneficial to the removal of phenol and catechol in wastewater.

2. EXPERIMENTAL AND COMPUTATIONAL DETAILS

2.1. Sample and Preparation. *2.1.1. Materials.* Graphite powder, 98% sulfuric acid, phosphorus pentoxide, potassium persulfate, potassium permanganate, 30% hydrogen peroxide, hydrochloric acid, $FeCl_2{\cdot}4H_2O$, $FeCl_3{\cdot}6H_2O$, sodium hydroxide, anhydrous ethanol, phenol, and catechol all are analytical pure. The water used in the experiment is deionized water.

2.1.2. Preparation. The details for the preparation of magnetic graphene oxides (MGOs) are shown in Figure 1. Graphene oxide adopts the improved Hummers method.[27] 4 g of graphite powder was added into the mixture of 15 mL of 98% concentrated H_2SO_4, 2.5 g of $K_2S_2O_8$, and 2.5 g of P_2O_5 for preoxidation, and the precipitate was obtained after standing, and the preoxidation product was dried at 50 °C. 1 g of the preoxidized product was weighed and oxidized in 36 mL of 98% concentrated H_2SO_4 and 5 g of potassium permanganate; then, the reactant was poured into deionized water and stirred, and 30% H_2O_2 was added drop by drop until the reactant appears bright yellow. After standing and layering, the golden liquid in the lower layer was taken out; 200 mL of hydrochloric acid solution with a mass fraction of 10% was added to wash many times and centrifugated at 10 000 R/min high speed until 1 mol/L $BaCl_2$ solution is added into the centrifuged supernatant without a white precipitate. After washing with deionized water many times, the pH of the

https://doi.org/10.1021/acsomega.3c09346
ACS Omega 2024, 9, 15101−15113

supernatant is about 7. The supernatant was removed and the black viscous solid obtained by high-speed centrifugation was put into an oven at 50 °C and then dried to get graphene oxide.

Fe_3O_4 nanoparticles were prepared by mixed coprecipitation. 0.5836 g of $FeCl_2{\cdot}4H_2O$ and 1 g of $FeCl_3{\cdot}6H_2O$ were weighed, 250 mL of water was added, and 0.5 mol/L NaOH solution was slowly added until the solution turned black and left for stratification. The black solution in the lower layer was washed with deionized water and anhydrous ethanol three times, and the black viscous product was dried in a 40 OC vacuum drying oven to obtain Fe_3O_4 nanoparticles.

Magnetic graphene oxide was prepared by the blending method.[28,29] 0.2 g of prepared Fe_3O_4 nanoparticles was weighed and 100 mL of deionized water was added; 0.5 g of prepared graphene oxide was weighed and 500 mL of deionized water was added. The above solutions were dissolved by ultrasonication at 40 kHz and stirred. The samples were centrifuged for 10 min in a high-speed centrifuge and dried at 30 °C.

2.2. Material Characterization. *2.2.1. FT-IR.* The Fourier transform infrared (FT-IR) spectra of MGOs were measured using a Fourier transform infrared spectrometer (Spectrum Two). The attenuated total reflection method was used with a scanning range of 4000−400 cm^{-1}, a resolution of 4 cm^{-1}, and 32 scans.

2.2.2. TEM. The transmission electron microscopy (TEM) pictures of MGOs were tested to analyze the morphological changes of the samples using a Tecnai G220 transmission electron microscope (FEI Corporation, USA). The sample was dispersed in ethanol and subjected to ultrasound. Then, the ethanol suspension containing the sample was dropped onto a copper mesh and placed in a sample chamber. The sample morphology was observed under a high-pressure vacuum environment of 120 V.

2.3. Adsorption Experiment. 2 mL of 0.256 mg/mL magnetic graphene oxide solution, 2 mL of 40 mg/L phenol or catechol solution were taken and mixed in a 5 mL closed centrifuge tube and placed in a constant-temperature water bath oscillator at 15 °C for absorption without light oscillation. In practical applications, such as wastewater treatment, phenol is toxic and may be more stable at lower temperatures, reducing experimental risks. Lower temperatures are more energy-efficient, and assessing adsorption performance at 15 °C allows the effectiveness of the adsorbent to be tested under more challenging conditions, giving insights into its range of performance and potential limitations. After appropriate time, the supernatant was filtered by a 0.45 um water filtration membrane. The absorbance of the obtained solution was measured at the maximum wavelength (phenol 270 nm, pyrocatechol 275 nm) by a UV spectrophotometer. The concentration of phenol and pyrocatechol in the solution was calculated according to the standard curve. The follow-up experiments were carried out according to similar methods. The adsorption capacity (q, mg/g) of phenol and catechol on magnetic graphene oxide is calculated according to the following equation

$$q = \frac{C_0 - C_1}{C(\mathrm{MOGs})} \quad (1)$$

where C_0 is the initial mass concentration of phenols in the solution (mg/mL), C_1 is the mass concentration of phenols after adsorption in the solution (mg/mL), and C(MGOs) is the mass concentration of magnetic graphene oxide (g/mL).

Considering that the volatilization of phenolic substances may affect the adsorption results in the laboratory, the volatilization of phenol and catechol at 25, 35, and 45 °C was tested, and relevant data are presented in the Adsorption Isotherm. The results showed that the volatility of phenol and catechol had no significant effect on the adsorption experiments.

2.4. Molecular Modeling Calculations Based on Quantum Mechanics. In this work, molecular simulation calculations based on quantum mechanics were carried out by using the self-consistent field molecular orbital (SCF-MO) method within the density functional theory (DFT) framework. The functional of DFT here was treated with BLYP with third-generation dispersion correction (BLYP-D3).[30−32] The main reason for this choice was that the adsorption of phenol and catechol on graphene in this study mainly involved noncovalent interactions.[33−35] The DFT BLYP-D3 method was previously reported to be able to obtain accurate molecular structure information for noncovalent assembly, and its accuracy value was even comparable to the high-precision *ab initio* method such as CCSD(T).[36,37] All geometric configuration optimizations and energy calculations were conducted with the Gaussian program at the 6-31G** basis set theory levels. In order to obtain a quantitative description of the different physical contributions of phenol and catechol adsorption on graphene, we also conducted energy decomposition analysis (EDA) calculations based on ADF at the DZP basis set level. In addition, in order to visually describe the adsorption area, strength, type, etc. of phenol and catechol on graphene, we also used the RDG method[38] and MUTILWFN program[39] to analyze the adsorption effect.

3. RESULTS AND DISCUSSION

3.1. Structure and Property of Magnetic Graphene Oxide Samples. The magnetic graphene oxide samples were characterized by TEM and FTIR. The layered structure and surface fold of graphene oxide can be clearly observed by TEM in Figure 2. In addition, the dark dot-like agglomerated

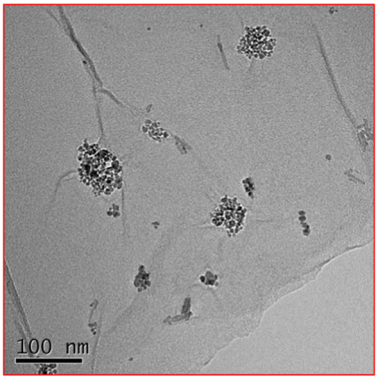

Figure 2. TEM images of MGOs.

particles in the figure are Fe_3O_4 nanoparticles, and their distribution shows obvious dispersion. TEM images show that magnetic nanoparticles are successfully loaded onto the surface of graphene oxide.

The FT-IR spectra before and after synthesis were compared, as shown in Figure 3. It can be seen from the

https://doi.org/10.1021/acsomega.3c09346
ACS Omega 2024, 9, 15101−15113

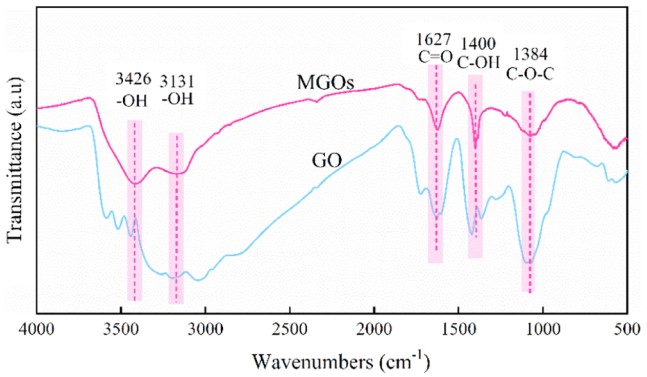

Figure 3. FT-IR spectra of MGOs.

spectrum that the broad peaks at 3426 and 3131 cm^{-1} have obvious vibration, which can be attributed to the −OH stretching vibration, the strong peaks at 1627 cm^{-1} come from the C═O carbonyl stretching vibration and the vibration is strengthened, and the peaks at 1400 and 1384 cm^{-1} come from C−OH and C−O−C stretching vibration, respectively, and have obvious displacement and change. There is an obvious peak at 581 cm^{-1}, which is contributed by the expansion vibration of Fe−O bonds. These characteristic peaks of FT-IR further prove that Fe_3O_4 nanoparticles and GOs are successfully compounded and the skeleton structure of GOs is not significantly affected before and after compounding.

3.2. Influence of Exposure Time. The effect of adsorption contact time on the adsorption of phenol and catechol on MGOs is shown in Figure 4. It can be seen that the adsorption contact time has a significant effect on the adsorption of phenol and acetone by MGOs. In the initial stage of adsorption, the adsorption rate was faster, and then, the adsorption rate decreased. The adsorption capacity of phenols increased with time, and the maximum adsorption capacity of phenol and catechol was reached at 60 min. After 60 min, the adsorption capacity decreased slightly, which may be caused by violent oscillation and prolonged time that the adsorbed phenols separated from the magnetic graphene oxide and returned to the solution. Therefore, 60 min was used as the adsorption equilibrium time to study the adsorption behavior and mechanism of magnetic graphene oxides for phenol and catechol. With the progress of the experiment, the optimal adsorption condition was reached at 60 min, after which the experiment continued and the adsorption trend decreased, so we believe that the peak was reached at 60 min in the experiment. This result was roughly consistent with the phenol adsorption capacity of the 3D N-doped graphene oxide aerogel prepared by Cui et al. in 2023, which gradually reached the maximum adsorption capacity in about 75 min.[25] This is the same as the adsorption equilibrium time used by Yang et al.[40] However, it takes 6 h for Yu[41] and Lee[42] to achieve adsorption equilibrium of phenol with reduced graphene oxide and aryl-functionalized reduced graphene oxide, respectively. Therefore, the adsorption equilibrium of magnetic graphene oxide is faster than that of graphene oxide.

It should be noted that the adsorption capacity of catechol by magnetic graphene oxide is up to 104.5 mg/g at 15 °C, while the adsorption capacity of phenol is only 18.4 mg/g under the same conditions, that is, the adsorption capacity of catechol is about 6 times that of phenol. The reason may be that there is one more hydroxyl in catechol than in phenol, which can enhance the interaction between phenols and MGOs.

3.3. Influence of Solution pH. The pH value of the solution changes the ionic state of the functional groups on the surface of the adsorption material and also affects the solubility, hydrophilicity, and degree of ionization of the adsorbate.[18] In this study, 0.2 mol/L NaOH or 0.2 mol/L hydrochloric acid was used to adjust the pH value of the solution to 2−9 to investigate the effect of the solution pH on the adsorption of phenols by magnetic graphene oxide. It can be seen from Figure 5 that when the solution pH rises from 2 to 6, the equilibrium adsorption capacity of phenol adsorbed by magnetic graphene oxide rises from 3.1 to 21.5 mg/g. When the pH of the solution exceeds 6, the equilibrium adsorption capacity decreases gradually. When the pH is 8 and 9, the equilibrium adsorption capacity is only about 9 mg/g. This shows that magnetic graphene oxide is suitable for phenol adsorption under weak acid conditions. The basic solution environment is not suitable for increasing the equilibrium adsorption capacity of phenol. Figure 5 shows the adsorption of catechol by graphene oxide on the right side with the pH value. When the pH value changes from 2 to 9, the adsorption trend of graphene oxide on catechol generally shows a downward trend, slowly decreasing at 2−4, and the pH value tends to be about 5−7, which basically remains stable. Finally, under alkaline conditions, that is, when the pH value reaches

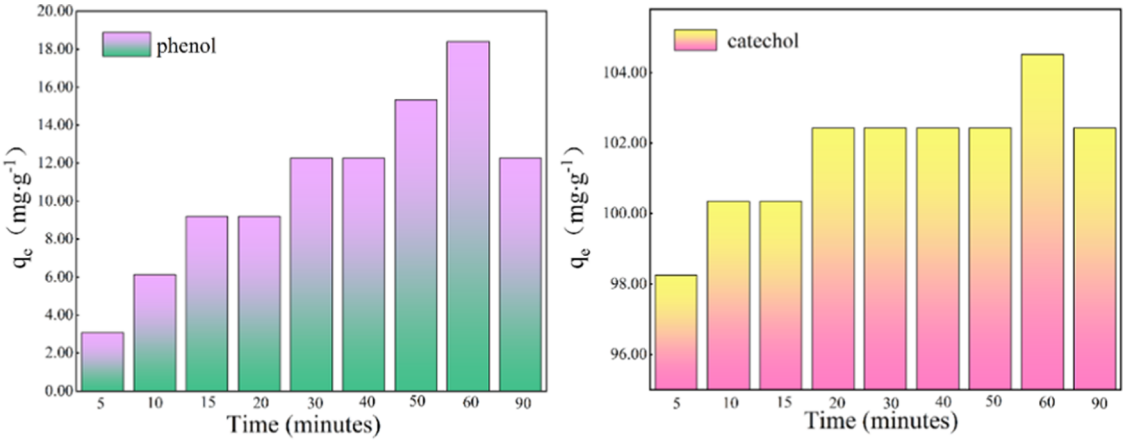

Figure 4. Adsorption of phenol (left) and catechol (right) by MGO with various contact times.

https://doi.org/10.1021/acsomega.3c09346
ACS Omega 2024, 9, 15101−15113

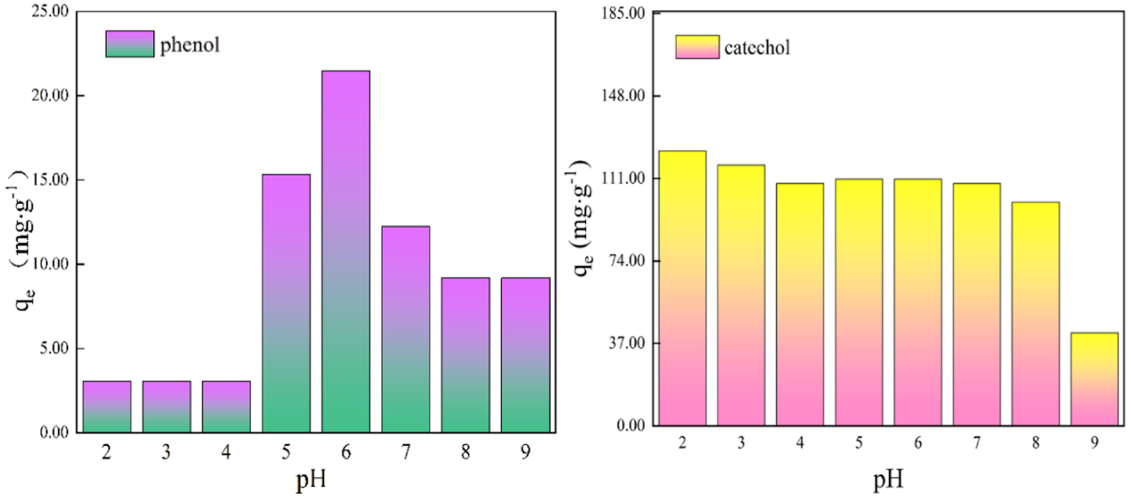

Figure 5. Adsorption of phenol (left) and catechol (right) by MGO at various pH values.

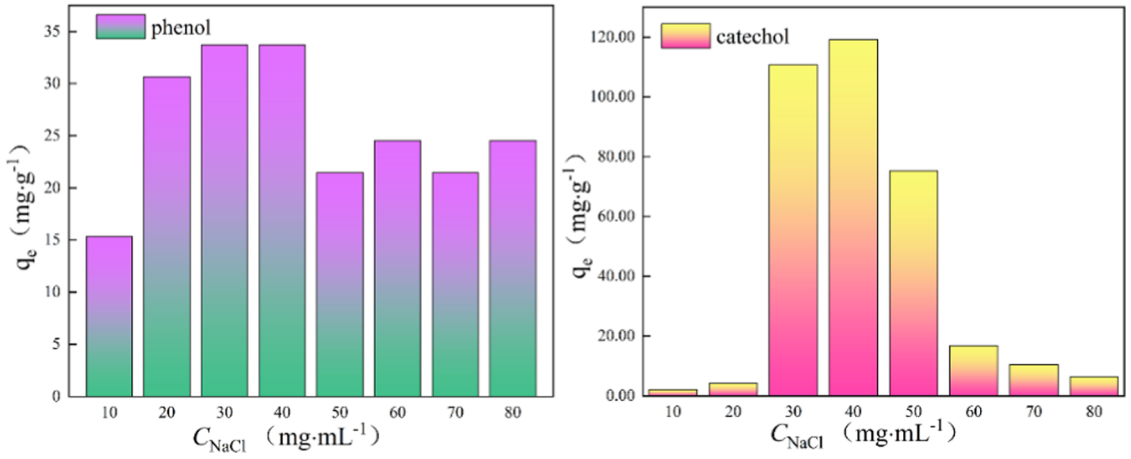

Figure 6. Adsorption of phenol and catechol by MGO with various ionic strengths.

8−9, the adsorption trend of graphene oxide on catechol generally remains stable. The adsorption capacity decreases rapidly. The whole range of adsorption capacity decreased from 123.3 to 100.3 mg/g, indicating that with increasing pH value, graphene oxide adsorption of catechol is unfavorable, it is not easy to improve the equilibrium adsorption capacity of catechol, and acidic conditions are the advantages of graphene oxide adsorption of catechol. This may be due to its rich oxygen-containing functional groups. Graphene oxide is negatively charged when dispersed in water. When the solution is alkaline, the amount of oxygen anion and negative charge density of graphene oxide and phenol or catechol increase; at this time, the electrostatic repulsion between the adsorbent and the adsorbent will reduce the effective adsorption between molecules, resulting in a reduction in adsorption capacity.[43] The change of pH value makes graphene oxide have an important effect on the adsorption capacity of phenol and catechol. GO is prone to protonation under acidic conditions, making GO's polycyclic aromatic network more hydrophobic, which contributes to the self-assembly of GO−water−GO. With the deepening of the protonation process, the more hydrophobic surface of GO nanoparticles is easy to be approached by adsorbents through hydrophobic interactions, thus promoting the development of $\pi-\pi$ interactions between the GO aromatic structure and adsorbents. However, when the pH value tends to be alkaline, due to the increase of electrostatic repulsion between phenol and catechol and the negatively charged GO surface and the electrostatic repulsion and hydrophobic interaction between phenol and catechol and the negatively charged adsorbent,[44] the removal efficiency of phenolic substances decreases under this alkaline condition. When Zhang et al. studied the removal of phenols from water by graphene oxide/manganese oxide composites in 2019, they believed that the oxidation potential under acidic conditions was stronger than that under alkaline conditions, resulting in stronger removal ability.[45] Zhao et al. studied the effect of the pH value on the removal of phenol from water medium by nitrogen-doped reduced graphene oxide. Similar results were found when the pH levels increased. When the pH value continues to increase from 8 to 10, the electrostatic interaction may not be the decisive factor in the adsorption process,[46] and the main adsorption mechanism may be the hydrogen bonding between the OH groups and the GO functional groups of phenol and catechol. Therefore, the removal efficiency decreases with the increase of the pH value.[47]

3.4. Influence of Ionic Strength. Inorganic salt ions often existing in wastewater will affect the dispersion of magnetic graphene oxide in aqueous solution and change the interaction between the adsorbent and adsorbate.[20] In this study, the effect of ionic strength on the adsorption of phenol and catechol by

https://doi.org/10.1021/acsomega.3c09346
ACS Omega 2024, 9, 15101−15113

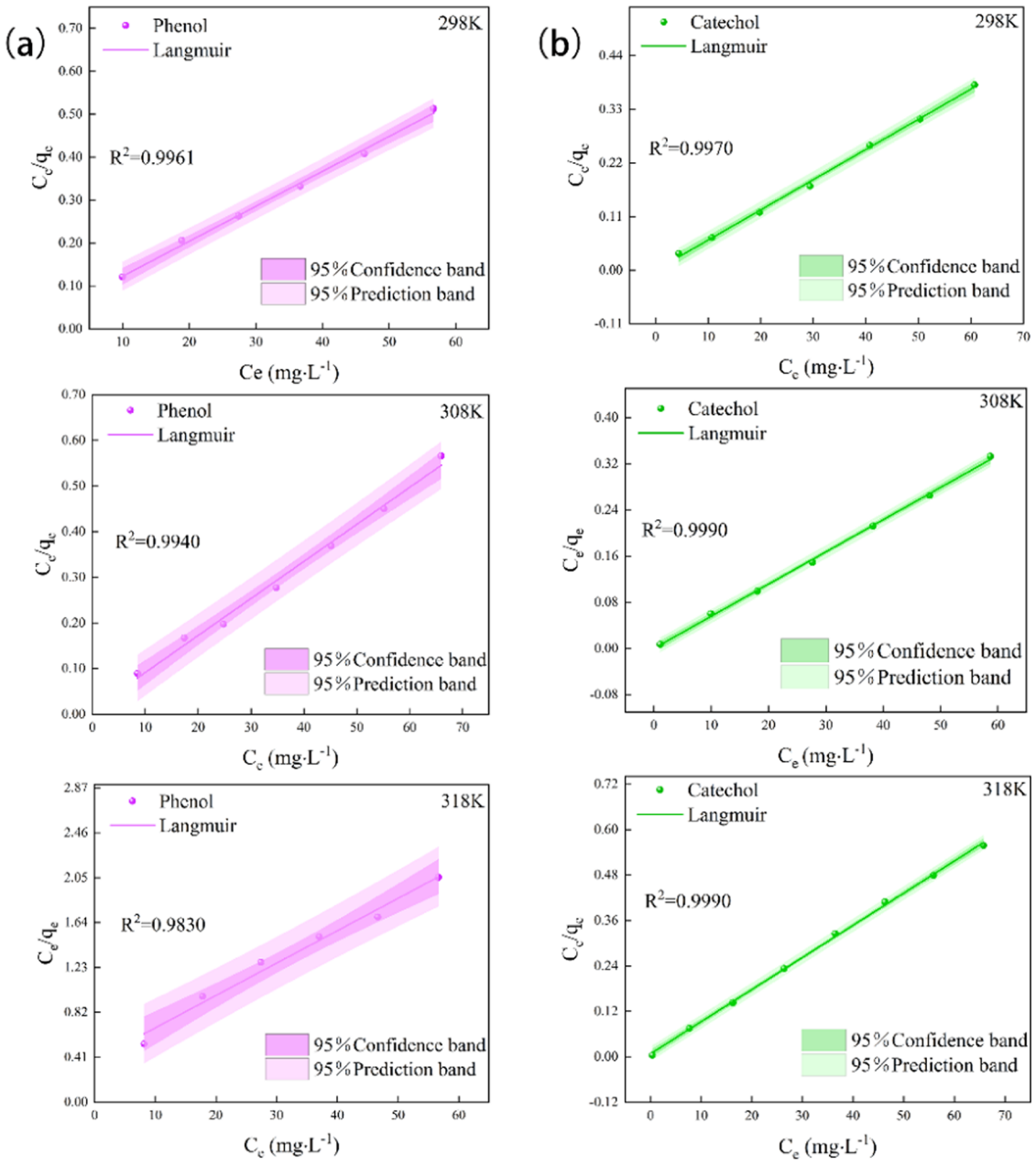

Figure 7. Adsorption isotherms of phenol (a) and catechol (b) adsorbed by MGO at various temperature.

magnetic graphene oxide was studied by adding different concentrations of NaCl solution. As shown in Figure 6, when the NaCl concentration increases from 10 to 40 mg/mL, the equilibrium adsorption capacity increases. When the salt concentration continues to increase, the equilibrium adsorption capacity shows a downward trend. When the concentration of NaCl is 30−40 mg/mL, magnetic graphene oxide has the best adsorption performance for phenol and catechol. The reason may be that phenol and catechol adhere together magnetically to the surface of graphene oxide in low salinity. With the increase of salinity, the double electric layer will be compressed and diffused, resulting in the reduction of the repulsion force and the increase of the adsorption capacity. A higher initial concentration means that there are more ions in the system to overcome the mass transfer resistance between the solution and the adsorbent,[48] thus absorbing more phenolic substances and promoting the adsorption process. If the salinity continues to increase, the electrostatic effect will have a significant effect on adsorption, which will weaken the attraction between phenol and magnetic GO. The adsorption site of the system adsorbent, that is, graphene oxide, reaches saturation, and the adsorption amount will no longer increase. The adsorption capacity of phenol and catechol decreased gradually when the ion concentration continued to rise, and the adsorption capacity became saturated with the increase in the initial concentration. The subsequent decline may be due to the excessive ion concentration in the system, which competed with phenol and catechol for adsorption,[49] thus inhibiting the increase of adsorption capacity and reducing the adsorption process.

3.5. Adsorption Isotherm. The adsorption isotherm is an important tool to describe the relationship between the equilibrium concentration of the solute in solution and the adsorption capacity of the adsorbent to the solute. The

https://doi.org/10.1021/acsomega.3c09346
ACS Omega 2024, 9, 15101−15113

Table 1. Correlative Parameters of the Langmuir Model of Phenol and Catechol on MGOs

	phenol				catechol			
T/K	q_m	k_L	R_L	R^2	q_m	k_L	R_L	R^2
298	123	0.196	0.34	0.996	161	77.5	<0.01	0.997
308	122	1.188	0.08	0.994	179	280	<0.01	0.999
318	34	0.077	0.56	0.983	118	1.06	0.01	0.999

adsorption behaviors of phenol and catechol at different temperatures (298, 308, and 318 K) and initial concentrations were investigated. Here, the Langmuir-type isotherm equation used for fitting data is

$$\frac{C_e}{q_e} = \frac{C_e}{q_m} + \frac{1}{(K_L \times q_m)} \quad (2)$$

$$R_L = \frac{I}{(1 + K_L C_o)} \quad (3)$$

where q_m is the maximum theoretical adsorption capacity of the adsorbent (mg/g), K_L (L/mg) is the Langmuir isotherm adsorption constant, and R_L is the dimensionless equilibrium parameter used to represent the nature of the adsorption process. When the R_L value is 0−1, it is favorable for adsorption. If the R_L value is greater than 1, it is unfavorable for adsorption. When the R_L value is equal to 1, the adsorption isotherm is linear or equal to zero, and the adsorption is irreversible.[50,51]

The adsorption isotherms of phenol and catechol on magnetic graphene oxide obtained by Langmuir-type isotherm equation fitting are shown in Figure 7, and the fitted data are shown in Table 1. It can be seen that temperature has a significant effect on the maximum equilibrium adsorption capacity: the maximum equilibrium adsorption capacity of MgO for phenol is 27.60 mg/g (318 K) < 113.44 mg/g (298 K) < 125.71 mg/g (308 K); the maximum equilibrium adsorption capacity of MgO for catechol is 117.90 mg/g (318 K) < 177.69 mg/g (298 K) < 186.89 mg/g (308 K). It can be seen that the maximum adsorption capacity of MgO for phenol and catechol increases from 298 to 308 K. However, the equilibrium adsorption decreased significantly when the temperature increased to 318 K. The possible reason is that initially, with the increase of temperature, the activity ability of the adsorbate increases and it is easier to reach the surface of MGOs. When the temperature is too high, the adsorption process may be exothermic, so the maximum equilibrium adsorption capacity decreases significantly.

The linear correlation coefficient R^2 of the adsorption of phenol and catechol by MGOs is above 0.98. Therefore, the Langmuir-type isothermal equation can well describe the adsorption behavior of phenol and catechol on magnetic graphene oxide. This shows that the adsorption of phenol and catechol on magnetic graphene oxide is mainly monolayer adsorption, that is, all adsorption sites are the same and the adsorbed phenols are independent of each other. The maximum R_L values of phenol and catechol are less than 0.56 and 0.01, respectively, which are obviously less than 1, so the adsorption is easy.

3.6. Adsorption Kinetics. In order to study the adsorption mechanism and possible speed control steps, it is very important to study the adsorption kinetics. In this study, the adsorption of phenol and catechol on magnetic graphene oxide was analyzed by mathematical models of the quasi-first-order kinetic model (eq 4), the quasi-second-order kinetics model (eq 5), the Weber−Morris model (eq 6), and the Elovich model (eq 7)

$$\ln(q_e - q_t) = \ln q_e - K_1 t \quad (4)$$

$$\frac{t}{q_t} = \frac{1}{K_2 q_e^2} + \frac{t}{q_e} \quad (5)$$

$$q_e = K_{id} \times t^{1/2} + C \quad (6)$$

$$q_e = \frac{1}{\beta}\ln(\alpha\beta) + \frac{1}{\beta}\ln t \quad (7)$$

Among them, K_1 (h^{-1}) and K_2 (g mg^{-1} min^{-1}) are the diffusion rate constants of quasi-first-order and quasi-second-order kinetics, respectively; q_e and q_t are the adsorption amount of phenols on magnetic graphene oxide (mg/g) at adsorption equilibrium or time t, respectively; K_{id} and C are the intraparticle diffusion rate constant ($mg{\cdot}g^{-1}{\cdot}min^{-0.5}$) and boundary layer constant, respectively; and α and β are the initial adsorption rate constant (g mg^{-1} min^{-1}) and desorption rate constant ($g{\cdot}mg^{-1}$), respectively. The adsorption kinetic fitting results of phenol and catechol are shown in Figure 8, and the calculated kinetic parameters are shown in Table 2.

It can be seen from Figure 8 that the quasi-first-order kinetic model of phenol adsorption has a good correlation, the correlation coefficient R^2 is 0.922, and the fitting effect is consistent with the actual situation. Moreover, the theoretical equilibrium adsorption (17.2 mg/g; see Table 2) predicted by the model is close to the actual equilibrium adsorption (18.4 mg/g). Therefore, the quasi-first-order kinetic model can well describe the adsorption kinetics of phenol on magnetic graphene oxide. This indicates that the adsorption rate of phenol is probably controlled by the diffusion step. For catechol, the fitting effect of the quasi-first-order kinetic model is not ideal, the correlation coefficient R^2 is only 0.751, and the predicted theoretical equilibrium adsorption capacity is also far from the actual equilibrium adsorption capacity. On the contrary, the quasi-second-order kinetic model of catechol adsorption has a good correlation, the correlation coefficient R^2 reaches 0.999, and the predicted theoretical equilibrium adsorption capacity (104.2 mg/g, see Table 2) is basically consistent with the actual equilibrium adsorption capacity (104.5 mg/g). Therefore, the quasi-second-order kinetic model can well describe the adsorption kinetics of catechol on magnetic graphene oxide. This indicates that the adsorption rate of catechol is likely to be controlled by the chemical adsorption mechanism, which involves electron sharing or electron transfer between the adsorbent and adsorbate.[52] The in-particle diffusion equation is used to reveal the rate-limiting steps. The result shows the linear part of the Weber-Morris diagram; the correlation coefficient R^2 is 0.6776. All the values of C representing the intercepts of Weber-Morris plots are nonzero.[53−55] According to the diffusion theory, it can be seen

https://doi.org/10.1021/acsomega.3c09346
ACS Omega 2024, 9, 15101−15113

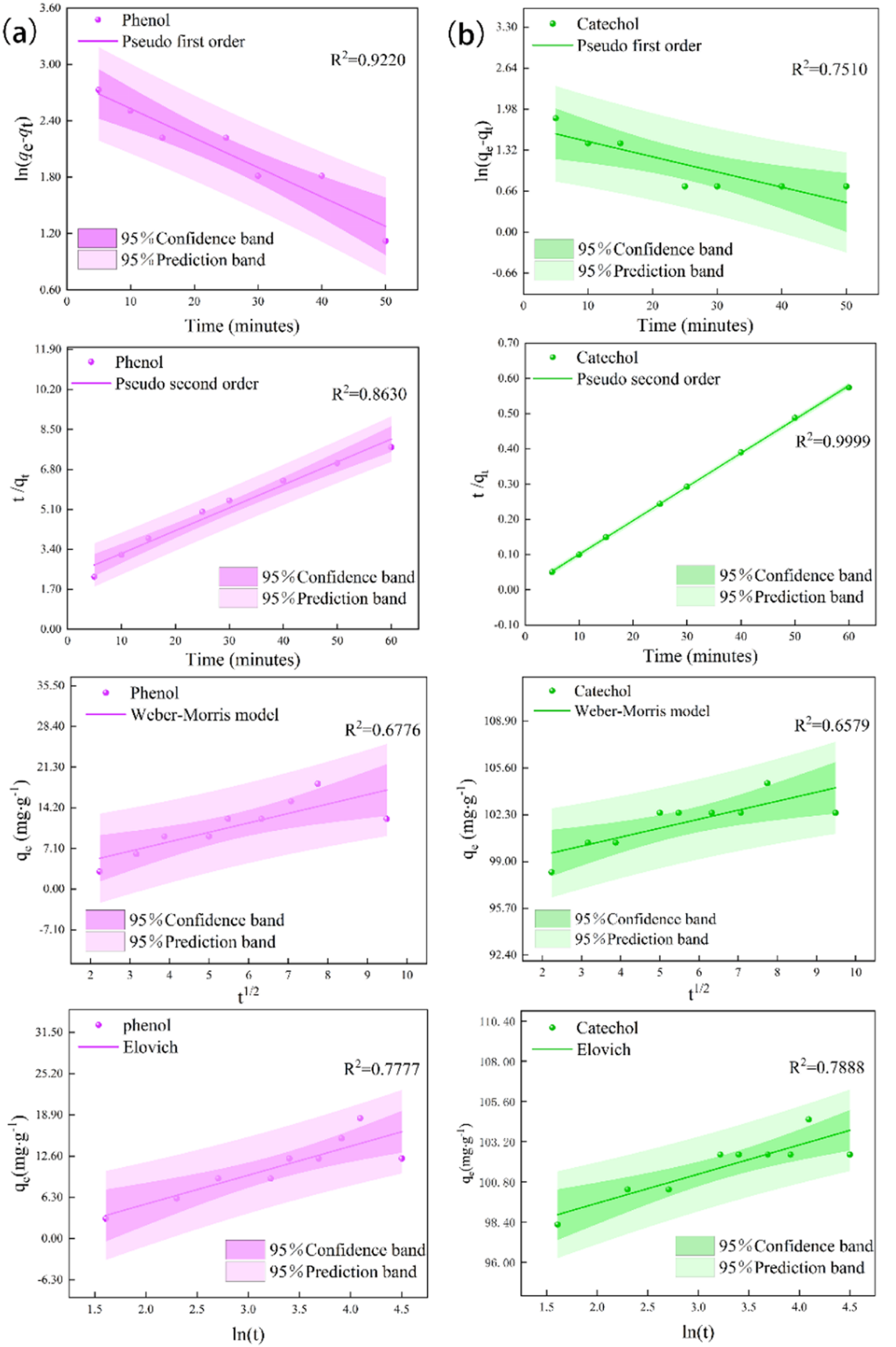

Figure 8. Four models of phenol (a) and catechol (b) adsorbed by MGOs.

that intraparticle diffusion is not the only factor affecting the adsorption, and the adsorption process roughly fits in one stage. This result is consistent with the experimental results; phenol and catechol adsorb faster during the 90 min study

https://doi.org/10.1021/acsomega.3c09346
ACS Omega 2024, 9, 15101−15113

Table 2. Correlative Parameters of Adsorption Kinetics of Phenol and Catechol on MGOs

	pseudo-first-order			pseudo-second-order			Weber-Morris			Elovich		
kinetic model	q_e	$k_{1(2)}$	R^2	q_e	$k_{1(2)}$	R^2	K_{id}	C	R^2	A	β	R^2
phenol	17.2	0.031	0.922	5.5	0.0246	0.751	1.6426	1.7068	0.678	1.976	0.226	0.778
catechol	27.6	0.001	0.863	104.2	0.0192	0.999	0.6332	98.190	0.658	1.48×10^{24}	0.574	0.789

period. The fitting results of the Elovich model show that the correlation coefficient R^2 is 0.777 and the diffusion rate determination step is less obvious.[56]

3.7. Quantum Chemical Insights into the Adsorptions. In order to understand and discuss the adsorption mechanism of phenol and catechol on the surface of graphene oxide at the microscale, we used quantum chemical methods based on DFT calculations to study the adsorption behavior of phenol and catechol on the surface of graphene oxide. We chose the $C_{114}H_{32}O_{20}$ nanosheet with a size of approximately 2.3 × 2.3 nm as the graphene oxide model for DFT calculations; the molecular structure model also includes typical oxygen-containing functional groups such as −OH, −COOH, and R−O−R, which are widely present in the structure of graphene oxide and play an important role in adsorption as reported in previous studies. The microstructure of oxidized graphene is characterized by defective graphene containing numerous oxygen-containing functional groups. The carbon atoms in the graphene oxide model we constructed maintain the highly conjugated structure of graphene, but there are structural defects at the edges and center. This structure also contains typical oxygen-containing functional groups such as −COOH, C−O−C, −OH, etc. These structural features are consistent with the microstructure model of graphene oxide reported in previous studies.[57,58] In addition, we also calculated the FT-IR spectra of the GO molecular structure model using the DFT method (Figure S1 in the Supporting Information). From Figure S1 in ESI, it can be seen that the infrared spectra obtained from DFT calculations are in good agreement with the peaks of the experiments, with only a slight difference in the intensity and peak position of the individual peaks. The difference of peak positions mainly reflects the displacements in the vibrational frequency of the calculated functional groups. This is because the FT-IR obtained by DFT is upon a single molecule structure of GO with excluding intramolecular interactions, which are indeed important for bulk materials of GO in experiments. The above results indicate that there is good correspondence between the calculated FT-IR spectra and the experimentally tested infrared spectra in Figure 3. This further confirms the rationality of the GO molecular structure.

In the DFT calculations, we attempted various different adsorption conformations as the initial structures. However, after molecular dynamics annealing calculations, it is found that the final stable adsorption conformation is mainly phenol and catechol adsorbed on graphene oxide in a manner in which the benzene ring is almost parallel to the graphene oxide nanosheets. The detailed structure is shown in Figure 9. Among them, the interaction distance between the benzene ring in phenol and catechol and graphene oxide nanosheets is approximately 3.2−3.5 Å, which is a noncovalent interaction distance. Moreover, the benzene ring overlaps above the six-membered ring in graphene. Therefore, phenol and catechol molecules exhibit typical $\pi-\pi$ interactions with graphene oxide in a stable adsorption configuration. In order to visually depict the interaction between phenol and catechol adsorbed on the surface of GO nanosheets, we used the RDG method to analyze the interaction region, strength, and type.[59−61] As shown in Figure 9, there is a significant electron density gradient change in the space between phenol or catechol on the surface of graphene oxide nanosheets, which is visual and direct evidence of the adsorption interaction in electronic structure theory. For phenol and catechol, the interaction regions given by RDG analysis are relatively close, mainly located in the spatial region of the adsorption site. However, due to the presence of more functional groups in catechol, the area of action is shown to be larger than that for phenol, which means that the intensity of interaction is stronger than that for phenol. It is also noticed that these interactions are mainly displayed in green color, which is an intuitive manifestation of the $\pi-\pi$ interaction. In addition, there is also an interaction display between the oxygen-containing functional groups on the surface of graphene oxide and the regions between phenol or catechol, with the color mainly marked as blue-green, which is a typical hydrogen bonding display. From the obtained structural analysis in Figure 9, the interaction distances between the hydrogen atom of the hydroxyl group in phenol and catechol and the oxygen atom in graphene oxide are 1.962 and 1.912 Å, respectively. These structural features and distances belong to typical hydrogen bonding interactions. Therefore, the adsorption of phenol and catechol on the surface of graphene oxide is not only $\pi-\pi$ stacking but also typical hydrogen bonding interactions.

In order to further quantitatively describe the physical essence of the adsorption of phenol and catechol on the surface of graphene oxide, we further used the energy decomposition analysis (EDA) method to calculate the adsorption effect. The results are shown in Table 3. The EDA results show that the interaction energy between phenol and graphene oxide is −0.938 eV, which is slightly larger than the −1.062 eV of catechol. This is consistent with the result mentioned in the RDG analysis that catechol exhibits a larger interaction area due to its more functional groups. Among the four energies decomposed by EDA, E_{pauli} is a positive value, which means that Pauli's contribution is not conducive to adsorption. The other three terms, namely, orbital interaction, electrostatic interaction, and dispersion interaction, are negative, which facilitate the surface adsorption of phenol and catechol on graphene oxide. Among these values in Table 3, one can find that the contribution of dispersion is the greatest among three negative components of EDA. Therefore, the adsorption of phenol and catechol on the surface of graphene oxide is mainly dominated by dispersion force. This is consistent with the significant electron density gradient changes during the adsorption of phenol and hydroquinone on the surface of graphene oxide nanosheets in the spatial region with $\pi-\pi$ stacking, as shown by RDG analysis. It should be pointed out that in addition to the dispersion effect, the numerical value of the electrostatic effect is also very important for stable adsorption, with the values of −0.835 and −1.028 eV for phenol and catechol, respectively. These values are less negative than that of the dispersion force by −1.326 and −1.455 eV for phenol and catechol, respectively. It is well

https://doi.org/10.1021/acsomega.3c09346
ACS Omega 2024, 9, 15101−15113

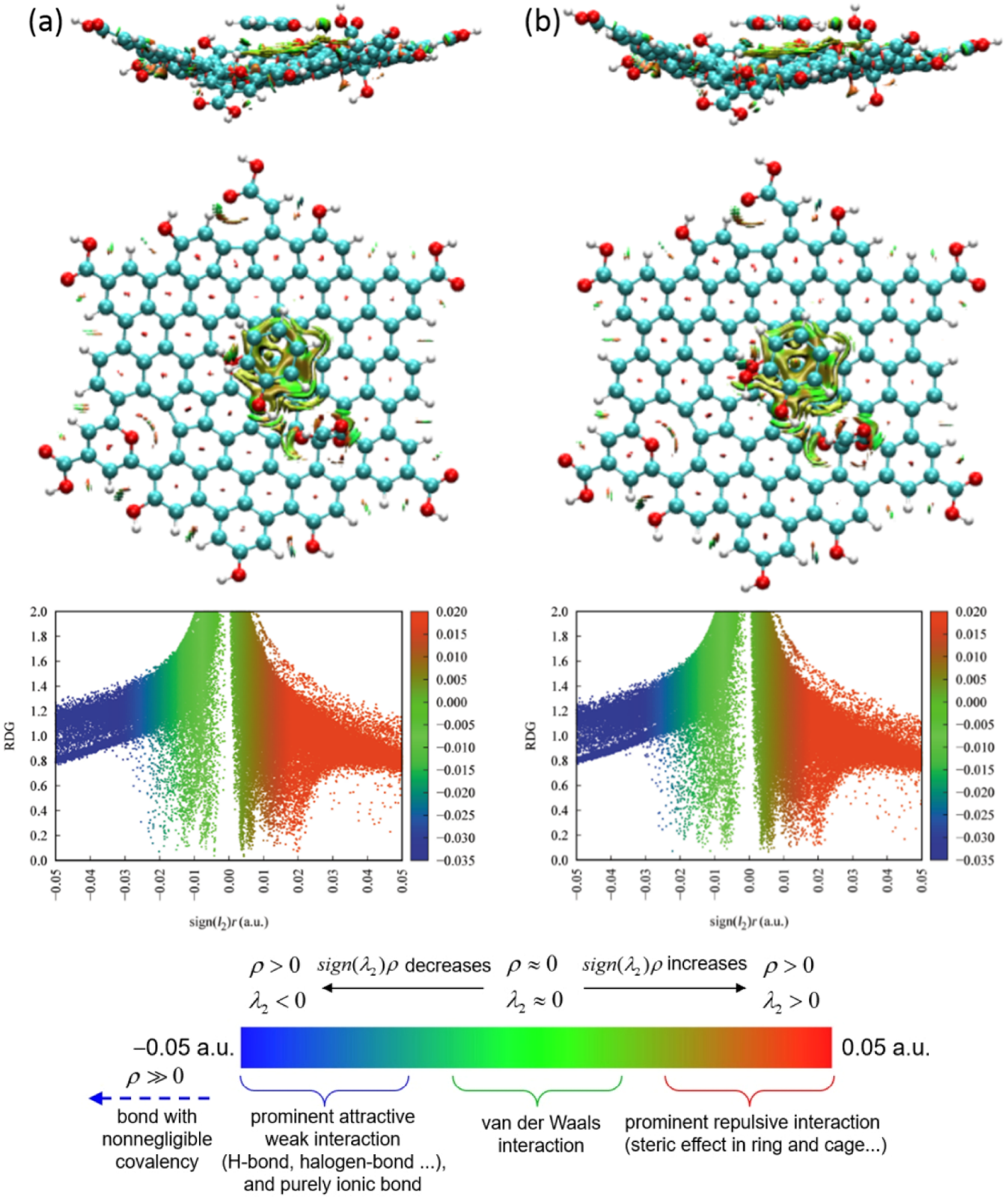

Figure 9. Structure and RDG interaction of phenol and catechol adsorbed on the surface of GOs nanosheets. (a) Phenol and (b) catechol.

known that the hydrogen bonding is considered to be dominated by electrostatic interactions in physical essence. This is also consistent with the fact that the hydrogen bonding interaction between phenol and catechol and the oxygen-containing functional groups on the surface of graphene oxide is observed in the stable adsorption structure as shown in RDG analysis. Besides, charge transfer is also studied for adsorption of phenol and catechol on the surface of graphene oxide. It is found that 0.0214 and 0.0202 *e* are transferred from phenol and catechol, respectively, to the graphene oxides. Thus, charge redistribution has occurred in adsorption of phenol and catechol on the surface of graphene oxide. This also could

https://doi.org/10.1021/acsomega.3c09346
ACS Omega 2024, 9, 15101−15113

Table 3. EDA Results of the Adsorption of Phenol and Catechol on the Surface of Graphene Oxide Nanosheets

molecule	E_{int} (eV)	E_{pauli} (eV)	E_{orb} (eV)	E_{elstat} (eV)	E_{disp} (eV)
phenol	−0.938	1.669	−0.448	−0.835	−1.326
catechol	−1.062	1.958	−0.537	−1.028	−1.455

enhance the interaction between phenol/catechol and graphene oxide, which agrees with the results of adsorption kinetics that the adsorption involves electron sharing or electron transfer, as mentioned above.

4. CONCLUSIONS

In summary, this work has prepared MGO composites by blending graphene oxide and Fe_3O_4 magnetic nanoparticles to remove phenol and catechol in wastewater. Various adsorption factors and adsorption mechanisms are discussed based on the experiments and DFT calculations. The main conclusions are as follows:

(1) The optimal process conditions for the adsorption of phenol and catechol on the surface of MGOs have been determined. The adsorption capacity of phenol and catechol increases with time but reached the maximum at 60 min. The ionic strength of inorganic salts will affect the adsorption of phenol and catechol by MGOs. MGOs are suitable for adsorption of phenol and catechol in weak acid conditions, and the alkaline solution environment is not conducive to increase the equilibrium adsorption capacity.

(2) The modes of adsorption isotherm for the adsorption of phenol and catechol on the surface of MGOs have been obtained. The results of the adsorption isotherm show that the Langmuir-type isotherm equation can well describe the adsorption behavior of phenol and catechol on MGOs. The adsorption is mainly on a single surface, and the adsorption is favorable.

(3) The modes of adsorption kinetics for the adsorption of phenol and catechol on the surface of MGOs have been explored. The adsorption of phenol on MGOs conforms to the quasi-first-order kinetic model, and the adsorption rate is likely to be controlled by the diffusion step. The adsorption of catechol on magnetic graphene oxide conforms to the quasi-second-order kinetic model, and the adsorption rate is likely to be controlled by the chemical adsorption mechanism.

(4) The mechanism and essence of the interaction of phenol and catechol on the surface of MGOs at the microscale have been revealed. Based on DFT calculations, it is found that phenol and catechol on the surfaces of graphene oxide nanosheets are in a noncovalent interaction distance. The interaction region, strength, and type between phenol/catechol and graphene oxide nanosheets could be directly pictured by the RDG analysis. Moreover, EDA results clearly demonstrated that the adsorption of phenol and catechol on the surface of graphene oxide is mainly dominated by dispersion force.

■ ASSOCIATED CONTENT

Supporting Information

The Supporting Information is available free of charge at https://pubs.acs.org/doi/10.1021/acsomega.3c09346.

Infrared spectrum obtained by the experiment and simulation (PDF)

■ AUTHOR INFORMATION

Corresponding Author

Hongcun Bai − *State Key Laboratory of High-efficiency Utilization of Coal and Green Chemical Engineering, College of Chemistry and Chemical Engineering, Ningxia University, Yinchuan, Ningxia 750021, China;* orcid.org/0000-0003-1747-6067; Email: hongcunbai@gmail.com, hongcunbai@nxu.edu.cn

Authors

Yuhua Wu − *State Key Laboratory of High-efficiency Utilization of Coal and Green Chemical Engineering, College of Chemistry and Chemical Engineering, Ningxia University, Yinchuan, Ningxia 750021, China*

Xi Zhang − *College of Basic Medical Sciences, Ningxia Medical University, Yinchuan 750004, China*

Caizhu Liu − *State Key Laboratory of High-efficiency Utilization of Coal and Green Chemical Engineering, College of Chemistry and Chemical Engineering, Ningxia University, Yinchuan, Ningxia 750021, China*

Lina Tian − *State Key Laboratory of High-efficiency Utilization of Coal and Green Chemical Engineering, College of Chemistry and Chemical Engineering, Ningxia University, Yinchuan, Ningxia 750021, China*

Yufan Zhang − *State Key Laboratory of High-efficiency Utilization of Coal and Green Chemical Engineering, College of Chemistry and Chemical Engineering, Ningxia University, Yinchuan, Ningxia 750021, China*

Meilin Zhu − *College of Basic Medical Sciences, Ningxia Medical University, Yinchuan 750004, China*

Weiye Qiao − *College of Chemistry and Chemical Engineering, Xingtai University, Xingtai 054001, China*

Jianbo Wu − *State Key Laboratory of High-efficiency Utilization of Coal and Green Chemical Engineering, College of Chemistry and Chemical Engineering, Ningxia University, Yinchuan, Ningxia 750021, China*

Shu Yan − *State Key Laboratory of High-efficiency Utilization of Coal and Green Chemical Engineering, College of Chemistry and Chemical Engineering, Ningxia University, Yinchuan, Ningxia 750021, China*

Hui Zhang − *State Key Laboratory of High-efficiency Utilization of Coal and Green Chemical Engineering, College of Chemistry and Chemical Engineering, Ningxia University, Yinchuan, Ningxia 750021, China;* orcid.org/0000-0003-2171-4881

Complete contact information is available at: https://pubs.acs.org/10.1021/acsomega.3c09346

Author Contributions

‖Y.W. and X.Z. contributed equally to this work.

Notes

The authors declare no competing financial interest.

■ ACKNOWLEDGMENTS

This work was mainly supported by the Natural Science Foundation of Ningxia (No. 2023AAC03020), the Key R&D Projects of Ningxia (No. 2022BSB03075), and the NSFC (No. 21863008).

REFERENCES

(1) Khedri, D.; Hassani, A. H.; Moniri, E.; Panahi, H. A.; Khaleghian, M. Efficient removal of phenolic contaminants from wastewater samples using functionalized graphene oxide with thermo-sensitive polymer: Adsorption isotherms, kinetics, and thermodynamics studies. *Surf. Interfaces* **2022**, *35*, No. 102439.

(2) Feng, J.; Ran, J.; Tao, M.; Zhang, W. Selective and Adjustable Removal of Phenolic Compounds from Water by Biquaternary Ammonium Polyacrylonitrile Fibers. *ACS Omega* **2021**, *6* (29), 18836−18847.

(3) Chen, Z.; Oh, W. D.; Yap, P. S. Recent advances in the utilization of immobilized laccase for the degradation of phenolic compounds in aqueous solutions: A review. *Chemosphere* **2022**, *307* (3), No. 135824.

(4) Wei, G. X.; Pan, G. B.; Wan, L. J.; Zhao, J. C.; Bai, C. L. In situ STM of phenolic compounds on Cu(111) in solution. *Surf. Sci.* **2002**, *520* (1−2), L625−L632.

(5) Chen, Y.; He, J.; Wang, Y. Q.; Kotsopoulos, T. A.; Kaparaju, P.; Zeng, R. J. Development of an anaerobic co-metabolic model for degradation of phenol, m-cresol and easily degradable substrate. *Biochem. Eng. J.* **2016**, *106*, 19−25.

(6) Salehi, S.; Abdollahi, K.; Panahi, R.; Rahmanian, N.; Shakeri, M.; Mokhtarani, B. Applications of Biocatalysts for Sustainable Oxidation of Phenolic Pollutants: A Review. *Sustainability* **2021**, *13* (15), 8620.

(7) Cai, W.; Wang, H.; Yang, Q. G.; Liu, T.; Wang, Y. Extracting phenolic compounds from aqueous solutions by cyclohexanone, a highly efficient extractant. *J. Ind. Eng. Chem.* **2022**, *116*, 393−399.

(8) Sun, H.; Yao, J.; Li, D.; Li, Q.; Liu, B.; Liu, S.; Feng, C.; et al. Removal of phenols from coal gasification wastewater through polypropylene hollow fiber supported liquid membrane. *Chem. Eng. Res. Des.* **2017**, *123*, 277−283.

(9) Li, D.; Cheng, Y.; Zuo, H.; Zhang, W.; Pan, G.; Fu, Y.; Wei, Q. Dual-functional biocatalytic membrane containing laccase-embedded metal-organic frameworks for detection and degradation of phenolic pollutant. *J. Colloid Interface Sci.* **2021**, *603*, 771−782.

(10) Mohamed, A.; Nasser, W. S.; Kamel, B. M.; Hashem, T. Photodegradation of phenol using composite nanofibers under visible light irradiation. *Eur. Polym. J.* **2019**, *113*, 192−196.

(11) Swain, G.; Sonwani, R. K.; Giri, B. S.; Singh, R. S.; Jaiswal, R. P.; Rai, B. N. Collective removal of phenol and ammonia in a moving bed biofilm reactor using modified bio-carriers: Process optimization and kinetic study. *Bioresour. Technol.* **2020**, *306*, No. 123177.

(12) Asghar, F.; Shakoor, B.; Fatima, S.; Munir, S.; Razzaq, H.; Naheed, S.; Butler, I. S. Fabrication and prospective applications of graphene oxide-modified nanocomposites for wastewater remediation. *RSC Adv.* **2022**, *12*, 11750.

(13) Pachamuthu, M. P.; Karthikeyan, S.; Maheswari, R.; Lee, A. F.; Ramanathan, A. Fenton-like degradation of Bisphenol A catalyzed by mesoporous Cu/TUD-1. *Appl. Surf. Sci.* **2017**, *393*, 67−73.

(14) Zhong, N.; Yuan, J.; Luo, Y.; Zhao, M.; Luo, B.; Liao, Q.; Rittmann, B. E.; et al. Intimately coupling photocatalysis with phenolics biodegradation and photosynthesis. *Chem. Eng. J.* **2021**, *425*, No. 130666.

(15) Graa, N. S.; Rodrigues, A. E. The Combined Implementation of Electrocoagulation and Adsorption Processes for the Treatment of Wastewaters. *Clean Technol.* **2022**, *4* (4), 1020−1053.

(16) Dai, J.; Li, Z. An equilibrium approach towards sustainable operation of a modern coal chemical industrial park. *Omega* **2023**, *120*, 102914.

(17) Khalil, K. M. S.; Khairy, M.; Allam, O. A. S.; Khalil, M. K. Formation of improved activated carbons from sugarcane bagasse as environmental materials for adsorption of phenolic pollutants. *Int. J. Environ. Sci. Technol.* **2022**, *19* (4), 3103−3116.

(18) Yagmur, E.; Turkoglu, S.; Banford, A.; Aktas, Z. The relative performance of microwave regenerated activated carbons on the removal of phenolic pollutants. *J. Cleaner Prod.* **2017**, *149* (15), 1109−1117.

(19) Idris, Z. M.; Dzahir, M. I. H. M.; Jamal, P.; Barkat, A. A.; Xian, R. L. W. Purification of bioactive phenolics from *Phanerochaete chysosporium* biomass extract on selected macroporous resins. *IOP Conf. Ser.: Mater. Sci. Eng.* **2017**, *206*, No. 012070.

(20) Motaee, A.; Javadian, S.; Khosravian, M. Influence of Adsorption Energy in Graphene Production via Surfactant-Assisted Exfoliation of Graphite: A Graphene-Dispersant Design. *ACS Appl. Nano Mater.* **2021**, *4* (4), 3545−3556.

(21) Wang, C.; Ou, L. Graphene oxide as a potential carrier or remover for flotation collectors: A molecular dynamics study. *Surf. Sci.* **2023**, *736*, No. 122334.

(22) Sarker, F.; Karim, N.; Afroj, S.; Koncherry, V.; Novoselov, K. S.; Potluri, P. High-Performance Graphene-Based Natural Fiber Composites. *ACS Appl. Mater. Interfaces* **2018**, *10* (40), 34502−34512.

(23) Hernández, L.; Augusto, P. A.; Castelo-Grande, T.; Barbosa, D. Regeneration and reuse of magnetic particles for contaminant degradation in water. *J. Environ. Manage.* **2021**, *285*, No. 112155.

(24) Fang, Z.; Gao, Y.; Wu, X.; Xu, X.; Sarmah, A. K.; Bolan, N.; Wang, H.; et al. A critical review on remediation of bisphenol S (BPS) contaminated water: Efficacy and mechanisms. *Crit. Rev. Environ. Sci. Technol.* **2020**, *50* (5), 476−522.

(25) Cui, Y.; Kang, W.; Hu, J. Effectiveness and mechanisms of the adsorption of phenol from wastewater onto N-doped graphene oxide aerogel. *J. Water Process Eng.* **2023**, *53*, 103665.

(26) Vunain, E.; Houndedjihou, D.; Monjerezi, M.; Muleja, A. A.; Kodom, B. Adsorption, kinetics and equilibrium studies on removal of catechol and resorcinol from aqueous solution using low-cost activated carbon prepared from sunflower (*Helianthus annuus*) seed hull residues. *Water, Air, Soil Pollut.* **2018**, *229*, No. 366, DOI: 10.1007/s11270-018-3993-9.

(27) Chen, X.; Qu, Z.; Liu, Z.; Ren, G. Mechanism of Oxidization of Graphite to Graphene Oxide by the Hummers Method. *ACS Omega* **2022**, *7* (27), 23503−23510.

(28) Doustkhah, E.; Rostamnia, S. Covalently bonded sulfonic acid magnetic graphene oxide: Fe3O4@GO-Pr-SO3H as a powerful hybrid catalyst for synthesis of indazolophthalazinetriones. *J. Colloid Interface Sci.* **2016**, *478*, 280−287.

(29) Mondal, J.; Nguyen, K. T.; Jana, A.; Kurniawan, K.; Borah, P.; Zhao, Y.; Bhaumik, A. Efficient alkene hydrogenation over a magnetically recoverable and recyclable Fe3O4@GO nanocatalyst using hydrazine hydrate as the hydrogen source. *Chem. Commun.* **2014**, *50* (81), 12095−12097.

(30) Barbosa, N.; Pagliai, M.; Sinha, S.; Barone, V.; Alfè, D.; Brancato, G. Enhancing the Accuracy of Ab Initio Molecular Dynamics by Fine Tuning of Effective Two-Body Interactions: Acetonitrile as a Test Case. *J. Phys. Chem. A* **2021**, *125* (48), 10475−10484.

(31) Diaz-Flores, P. E.; López-Urı, F.; Terrones, M.; Rangel-Mendez, J. R. Simultaneous adsorption of Cd^{2+} and phenol on modified N-doped carbon nanotubes: experimental and DFT studies. *J. Colloid Interface Sci.* **2009**, *334*, 124−131.

(32) Mandeep; Sharma, L.; Kakkar, R. DFT study on the adsorption of p-nitrophenol over vacancy and Pt-doped graphene sheets. *Comput. Theor. Chem.* **2018**, *1142*, 88−96.

(33) de Moraes, E. E.; Tonel, M. Z.; Fagan, S. B.; Barbosa, M. C. Density functional theory study of π-aromatic interaction of benzene, phenol, catechol, dopamine isolated dimers and adsorbed on graphene surface. *J. Mol. Model.* **2019**, *25* (10), No. 302.

(34) Zhan, J.; Lei, Z.; Zhang, Y. Non-covalent interactions of graphene surface: Mechanisms and applications. *Chem* **2022**, *8*, 947−979.

(35) Banerjee, S.; Rappe, A. M. Mechanochemical Molecular Motion Using Noncovalent Interactions on Graphene and Its Application to Tailoring the Adsorption Energetics. *ACS Mater. Lett.* **2023**, *5* (2), 574−579.

(36) Su, H.; Wu, Q.; Wang, H.; Wang, H. An assessment of the random-phase approximation functional and characteristics analysis for noncovalent cation−π interactions. *Phys. Chem. Chem. Phys.* **2017**, *19* (38), 26014−26021.

https://doi.org/10.1021/acsomega.3c09346
ACS Omega 2024, 9, 15101−15113

(37) Caldeweyher, E.; Bannwarth, C.; Grimme, S. Extension of the D3 dispersion coefficient model. *J. Chem. Phys.* **2017**, *147* (3), No. 034112.
(38) Wu, P.; Chaudret, R.; Hu, X.; Yang, W. Noncovalent interaction analysis in fluctuating environments. *J. Chem. Theory Comput.* **2013**, *9* (5), 2226−2234.
(39) Lu, T.; Chen, F. Multiwfn: A multifunctional wavefunction analyzer. *J. Comput. Chem.* **2012**, *33* (5), 580−592.
(40) Yang, X. X.; Luo, D. M. Study on phenol adsorption characteristics of modified semi-coke. *Speciality Petrochem.* **2017**, *34* (1), 47−50.
(41) Yu, S.; Wang, X.; Yao, W.; Wang, J.; Ji, Y.; Ai, Y.; Wang, X.; et al. Macroscopic, spectroscopic and theoretical investigation for the interaction of phenol and naphthol on reduced graphene oxide. *Environ. Sci. Technol.* **2017**, *51*, 3278−3286.
(42) Lee, S.; Moon, B. J.; Lee, H. J.; Bae, S.; Kim, T. W.; Jung, Y. C.; Park, J. H.; Lee, S. H. Enhancement of adsorption performance for organic molecules by combined effect of intermolecular interaction and morphology in porous rGO-incorporated hydrogels. *ACS Appl. Mater. Interfaces* **2018**, *10*, 17335−17344.
(43) Konicki, W.; Aleksandrzak, M.; Mijowska, E. Equilibrium, kinetic and thermodynamic studies on adsorption of cationic dyes from aqueous solutions using graphene oxide. *Chem. Eng. Res. Des.* **2017**, *123*, 35−49.
(44) Al-Ghouti, M. A.; Sayma, J.; Munira, N.; Mohamed, D.; Da'na, D. A.; Qiblawey, H.; Alkhouzaam, A. Effective removal of phenol from wastewater using a hybrid process of graphene oxide adsorption and UV-irradiation. *Environ. Technol. Innovation* **2022**, *27*, No. 102525.
(45) Zhang, B.; Zhao, R.; Sun, D.; Li, Y.; Wu, T. Sustainable fabrication of graphene oxide/manganese oxide composites for removing phenolic compounds by adsorption-oxidation process. *J. Cleaner Prod.* **2019**, *215*, 165−174.
(46) Zhao, R.; Li, Y.; Ji, J.; Wang, Q.; Li, G.; Wu, T.; Zhang, B. Efficient removal of phenol and p-nitrophenol using nitrogen-doped reduced graphene oxide. *Colloids Surf., A* **2021**, *611*, No. 125866.
(47) Parvin, N.; Babapoor, A.; Nematollahzadeh, A.; Mousavi, S. M. Removal of phenol and β-naphthol from aqueous solution by decorated graphene oxide with magnetic iron for modified polyrhodanine as nanocomposite adsorbents: Kinetic, equilibrium and thermodynamic studies. *React. Funct. Polym.*. **2020***156* 104718.
(48) Ai, L.; Zhang, C.; Liao, F.; Wang, Y.; Li, M.; Meng, L.; Jiang, J. Removal of methylene blue from aqueous solution with magnetite loaded multi-wall carbon nanotube: kinetic, isotherm and mechanism analysis. *J. Hazard. Mater.* **2011**, *198*, 282−290.
(49) Xu, X.; Li, P.; Yang, S.; Zhang, T.; Han, X.; Zhou, G.; Cao, Y.; Teng, D. The performance and mechanism of a Mg-Al double-layer oxide in chloride ion removal from an aqueous solution. *Nanomaterials* **2022**, *12*, 846 DOI: 10.3390/nano12050846.
(50) Ulatowska, J.; Stala, U.; Polowczyk, I. Comparison of Cr(VI) Adsorption Using Synthetic Schwertmannite Obtained by Fe^{3+} Hydrolysis and Fe^{2+} Oxidation: Kinetics, Isotherms and Adsorption Mechanism. *Int. J. Mol. Sci.* **2021**, *22* (15), 8175.
(51) Zhou, Y.; Zhang, X.; Deng, J.; Li, C.; Sun, K.; Luo, X.; Yuan, S. Adsorption and mechanism study for phenol removal by 10% CO2 activated bio-char after acid or alkali pretreatment. *J. Environ. Manage.* **2023**, *348*, No. 119317.
(52) Tekin, N.; Safakli, A.; Bingol, D. Process modeling and thermodynamics and kinetics evaluation of Basic Yellow 28 adsorption onto sepiolite. *Desalin. Water Treat.* **2015**, *54* (7), 2023−2035.
(53) Xiang, L.; Xiao, T.; Mo, C. H.; Zhao, H. M.; Li, Y. W.; Li, H.; Wong, M. H.; et al. Sorption kinetics, isotherms, and mechanism of aniline aerofloat to agricultural soils with various physicochemical properties. *Ecotoxicol. Environ. Saf.* **2018**, *154*, 84−91.
(54) Lu, T.; Xue, C.; Shao, J.; Gu, J. D.; Zeng, Q.; Luo, S. Adsorption of dibutyl phthalate on Burkholderia cepacia, minerals, and their mixtures: Behaviors and mechanisms. *Int. Biodeterior. Biodegrad.* **2016**, *114*, 1−7.
(55) Marco-Brown, J. L.; Guz, L.; Olivelli, M. S.; Schampera, B.; Sánchez, R. T.; Curutchet, G.; Candal, R. New insights on crystal violet dye adsorption on montmorillonite: Kinetics and surface complexes studies. *Chem. Eng. J.* **2018**, *333*, 495−504.
(56) Li, G.; Zhu, W.; Zhu, L.; Chai, X. Effect of pyrolytic temperature on the adsorptive removal of p-benzoquinone, tetracycline, and polyvinyl alcohol by the biochars from sugarcane bagasse. *Korean J. Chem. Eng.* **2016**, *33*, 2215−2221.
(57) Feng, W.; Li, Z.; Gao, H.; Wang, Q.; Bai, H.; Li, P. Understanding the molecular structure of HSW coal at atomic level: A comprehensive characterization from combined experimental and computational study. *Green Energy Environ.* **2021**, *6* (1), 150−159.
(58) Wang, Q.; Zhang, J.; Li, H.; Zhang, H.; Bai, H.; Guo, Q. Exploring molecular structure characteristics and chemical index of Qinghua bituminous coal: A comprehensive insight from single molecule of macerals to particles with various sizes. *Powder Technol.* **2022**, *396*, 36−49.
(59) Sajid, H.; Ayub, K.; Mahmood, T. Sensing behaviour of monocyclic C18 and B9N9 analogues toward chemical warfare agents (CWAs); quantum chemical approach. *Surf. Interfaces* **2022**, *30*, No. 101912.
(60) Gao, H.; Qiao, W.; Zhu, M.; Wu, J.; Zhang, X.; Yan, W.; Li, Y.; et al. First-principle insights into the non-covalent interaction between nucleotide bases and flat nanocarbon: Graphene vs graphdiyne. *Diamond Relat. Mater.* **2023**, *139*, No. 110366.
(61) Zhang, Z.; Qiao, W.; Zhu, M.; Meng, L.; Yan, S.; Feng, R.; Li, Y.; et al. The interaction between nucleotide bases and nano carbon: The dimension dominates. *Surf. Interfaces* **2023**, *37*, No. 102715.

https://doi.org/10.1021/acsomega.3c09346
ACS Omega 2024, 9, 15101−15113